J Mater Sci: Mater Electron **(2024) 35:707**

Sustainable formaldehyde-free copper electroless plating on carbon-epoxy substrates

Mario Bragaglia[1,*], Lorenzo Paleari[1], Matteo Mariani[1], and Francesca Nanni[1]

[1] *Department of Enterprise Engineering, University of Rome "Tor Vergata", Mario Lucertini", and INSTM RU Roma—Tor Vergata, Via del Politecnico 1, 00133 Rome, Italy*

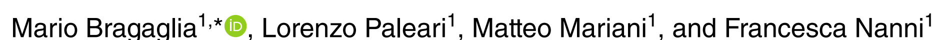

Received: 24 December 2023
Accepted: 30 March 2024
Published online:
4 April 2024

© The Author(s), 2024

ABSTRACT

In this paper, a formaldehyde-free copper electroless plating process was optimized using statistical analysis (Design of Experiment) in order to maximize the adhesion and the electrical conductivity when deposited on carbon-epoxy substrates. The coatings' morphologies, the electrical resistance, and the adhesion vary significantly as function of electroless plating parameters, but among the selected processing parameters, (pH of the electroless solution, temperature, concentration of reducing agent (glyoxylic acid), and concentration of complexing agent (EDTA)) only the temperature and the concentration of the reducing agent resulted to be influencing factors for the deposition process. A multi-objective optimization approach allowed to set the electroless process parameters in order to obtain optimized coatings presenting improved adhesion (scratch test's critical load CL3 > 30 N) and electrical conductivity (Rs = 1.91×10^{-2} Ω/sq).

1 Introduction

Polymer and polymer composites are characterized by a significantly lower density compared to metals which is an essential and attractive feature when operating in automotive, aeronautical, and space sectors. In particular, carbon fiber-reinforced polymers (CFRPs) composite materials made of carbon fibers and a polymer resin matrix are known for their high strength-to-weight ratio and are largely used in the manufacturing of aircraft components, wind turbine blades, and satellite components [1]. On the other hand, they are generally electrically insulators, and their use is excluded from a range of applications where electrical conductivity is needed, such as electronics, electromagnetic shielding, antennas, and waveguides.

Coating the polymeric material with a metallic (hence electrically conductive) layer is a possible answer for the use of CFRPs in all the applications that also require electrical conductivity. Among several coating techniques, the electroless coating process is one of the most used. Electroless process allows for the production of a metal deposition on non-conductive substrates, generating a continuous and uniform metallic coating [2]. As a wet chemical route, this coating technique offers several advantages: it is simple, reproducible, suitable for covering large area, it does not need a vacuum process, and lastly the process temperatures are low resulting in low energy consumption [3]. Moreover, other advantages are the possibility to coat substrates having complex geometries and a lower costs with respect to

Address correspondence to E-mail: bragaglia@ing.uniroma2.it

https://doi.org/10.1007/s10854-024-12493-9

other coating techniques [4]. In the electroless plating, the substrate is immersed in an aqueous solution which contains a salt of the metal to be deposited, along with a reducing agent, a complexing agent, a stabilizer, and a buffer system. The metallic ions and the reducing agent will react via a redox reaction so that the metal ions migrate to the substrate and nucleate a thin metallic layer without the application of an external electric voltage [5, 6]. Most deposited metals are copper (Cu) [7], nickel (Ni) [8], and silver (Ag) [2]. Electroless plating process consists of three main steps: (i) surface preparation of the substrate, (ii) surface catalytic activation, and (iii) electroless plating bath where the redox reactions take place forming the coating. The reducing agent is key factor for the electroless plating process: it is responsible, through its oxidation, for the reduction of the metal cation to the metallic form. In the electroless copper deposition, the most used reducing agent is formaldehyde (CH_2O) solution. The general reaction for the deposition of copper using CH_2O is reported in Eq. 1:

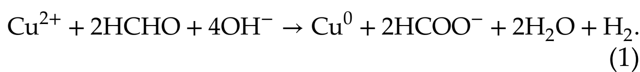

$$Cu^{2+} + 2HCHO + 4OH^- \rightarrow Cu^0 + 2HCOO^- + 2H_2O + H_2. \quad (1)$$

The activation energy for this reaction is 60 kJ/mol. This implies that the deposition temperature has to be higher than room temperature (RT = 25 °C). As a redox, two simultaneous reactions take place: the cathodic reaction is the reduction of the Cu ions to metallic form, while the anodic one is the oxidation of the formaldehyde which, in the case of highly alkaline solutions, dissociates through the Cannizzaro's reaction as follows (Eq. 2) [9]:

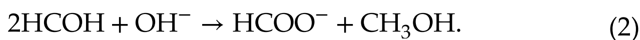

$$2HCOH + OH^- \rightarrow HCOO^- + CH_3OH. \quad (2)$$

Although the process is extremely efficient, formaldehyde is characterized by a high toxicity and a strong environmental impact [10]. It is known to be a respiratory and skin irritant and it can cause a range of health issues. Indeed, formaldehyde exposure has been linked to an increased risk of certain types of cancers, including nasopharyngeal cancer, sino-nasal cancer, and leukemia [11]. Due to its potential health risks, many countries have established regulatory limits on formaldehyde exposure both in workplaces and consumer products to protect public health and safety.

Less toxic compounds such as sodium hypophosphite (NaH_2PO_2), dimethylamine borane [12], and glyoxylic acid ($C_2H_2O_3$) have been recently studied as reducing agents for the electroless deposition of copper [13–15]. In particular, glyoxylic acid, a dicarboxylic acid having both a carboxyl group (–COOH) and an aldehyde group (-CHO), has proved to be a potential substitute of formaldehyde as reducing agent for the electroless deposition of copper [16, 17].

The redox reaction using $C_2H_2O_3$ as reducing agent is reported in Eq. 3:

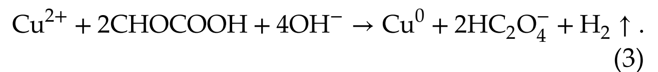

$$Cu^{2+} + 2CHOCOOH + 4OH^- \rightarrow Cu^0 + 2HC_2O_4^- + H_2 \uparrow . \quad (3)$$

Also in this case, the oxidation of glyoxylic acid follows the Cannizzaro's reaction reported in Eq. 4 and the final products are oxalate and glycolate [13]:

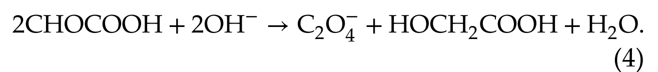

$$2CHOCOOH + 2OH^- \rightarrow C_2O_4^- + HOCH_2COOH + H_2O. \quad (4)$$

The Cannizzaro's reaction is faster when using glyoxylic acid than formaldehyde. In fact, the electroless process with glyoxylic acid as reducing agent is completely autocatalytic, while the aldehyde group of glyoxylic acid promotes hydrolysis, forming an intermediate product boosting the catalytic activity toward the reduction of Cu ions [9, 18]. Indeed, the deposition rate doubles (up to 6 µm/h) with the same concentration of metal ions and temperature of the solution with respect to the formaldehyde deposition bath. The electroless of copper is also a pH-dependent process: the metal deposition starts at a pH value of 11 but it has been shown that an increase of deposition rate happens in the pH range 12–14 [19]. At the same time, pH can influence the uniformity of the shining and the grain size of the coating [20]. Other factors that influence the deposition are the temperature [21] and the complexing agent. A complexing agent is an ion, molecule, or functional group that can bind with metal ions through one or more coordination bonds resulting in the formation of a complex [22]. This prevents the precipitation of copper as insoluble copper hydroxides or oxides keeping copper ions in solution and available for deposition. As the copper ions are consumed during the deposition process, complexing agents assist in replenishing the copper ions in the plating bath, helping to maintain a constant and effective source of copper for deposition. Among the complexing agents, the most used is ethylenediaminetetraacetic acid (EDTA) but other compounds such as sodium and potassium tartrate (Rochelle Salt), malic acid,

succinic acid, triethanolamine, and ethylenediamine have been investigated [14, 23].

Temperature on the other hand plays a crucial role in controlling the kinetics and properties of the deposition process. The rise in the bath temperature increases the reaction rate but at the same time it compromises the bath stability [24]. A temperature value of 70–75 °C is generally recognized as the upper limit for the temperature bath as higher temperature leads to the spontaneous decomposition of bath solution [25].

Many process variables are involved in the deposition process which results to be quite complex and a slight variation of the processing parameters can lead to unsuccessful results.

The aim of this work is the optimization of the copper electroless plating process on carbon fiber-reinforced laminates replacing toxic reagents with non-toxic ones (i.e., glyoxylic acid) in order to obtain a more sustainable process. A statistical approach (Design of Experiments, DoE) has been applied to identify and optimize the most influencing process parameters affecting the copper deposition (i.e., concentration of reducing agent, concentration of complexing agent, temperature, and pH). The produced coatings have been characterized from a chemical, electrical, and morphological point of view, while the optimization aimed at maximizing the coating adhesion and electrical conductivity, which were evaluated performing scratch tests and Van der Pauw measurements, respectively. The research introduces a novel approach in the electroless plating field, not only providing a systematic and efficient means to identify and optimize key process parameters but also emphasizing a broader commitment to ecological responsibility by replacing traditional toxic reagents, aligning with the growing demand for greener manufacturing processes.

2 Experimental

2.1 CFRP production and substrate sample preparation

Carbon-epoxy laminates (200 × 200 × 2 mm) in 0/90° stacking sequence configuration were produced using pre-pregs (XC130, wave 2 × 2 Twill, filament count 3 k, *Prepreg Carbon Fibre*) provided by *XPREG Easy Composites*. CFRPs were cured in autoclave by applying 7 bars of pressure at 120 °C for 1 h with a following post-cure treatment at 130 °C for 2 h.

Rectangular samples having dimension (15 × 20 × 2 mm) were cut out using a diamond saw (*Buehler* Isomet 4000 Linear Precision Saw) at 3500 rpm blade speed and 5 mm/min cut speed. Samples were washed in ethanol (*Sigma Aldrich*) and dried in oven at 50 °C prior to use.

2.2 Etching, pre-activation, and activation of CFRP substrates

A potassium hydroxide alcoholic solution was selected as the etching solution. Potassium hydroxide (KOH, *Carlo Erba Reagents*) was dissolved in ethanol (EtOH, *Sigma Aldrich*) with a concentration of 80 g/L. Samples have been immersed for 30 min and successively washed multiple times in distilled water and dried in oven (*Binder*) at 50 °C for 24 h.

The wettability of neat and etched substrate was assessed, following ASTM D 5946–04 standard, by measuring the static contact angle of a sessile distilled water droplet (8 μL) deposited on the surface through a Gilson pipette. A digital picture was acquired 30 s after dropping to ensure that the droplet reached its equilibrium position, and the contact angle has been measured through image analysis software (ImageJ). Static contact angle was calculated by applying Eq. 5:

$$\theta = 2tan^{-1}\left(\frac{H}{R}\right), \tag{5}$$

where H and R are the height and the radius of the drop, respectively.

A surface pre-activation in a Tin chloride-based solution was performed. For the preparation of the pre-activation solution, Tin (II) chloride dihydrate ($SnCl_2 \cdot 2H_2O$, *Sigma Aldrich*, assay > 99.99%) was mixed in distilled water (dH_2O) in the H_2O: $SnCl_2 \cdot 2H_2O$ molar ratio of 100: 0.05. Hydrochloric acid (HCl, 37%, *Carlo Erba Reagents*) in the H_2O: HCl molar ratio 100: 0.5 was added to the mixture contained in a glass beaker at room temperature under constant magnetic stirring. CFRP etched substrates have been immersed in the prepared solution for 30 min and then washed in distilled water and dried (24 h, 50 °C).

The selected catalytically activation solution involves silver as activator. The solution has been prepared as follows: dH_2O, ammonia solution (NH_3, *Carlo Erba Reagents*), silver nitrate ($AgNO_3$, *Sigma Aldrich* > 99.0%), and ammonium sulfate ($(NH_4)2SO_4$,

Sigma Aldrich > 99.0%) were mixed together in a glass beaker at room temperature (RT) in the H_2O: NH_3: ($(NH_4)2SO_4$): ($AgNO_3$) molar ratio 14: 2: 0.1: 0.002. Samples were dipped in the activation solution for 1 min and successively washed in dH_2O and dried at 50 °C for 24 h.

2.3 Design of experiment (DoE) for the Cu electroless deposition

The electroless plating bath was prepared as follows: anhydrous copper (II) sulfate ($CuSO_4$, *Carlo Erba Reagents*) was dissolved in distilled water in the concentration of 0.37 M. Glyoxylic acid ($C_2H_2O_3$, *Sigma Aldrich*) was added as reducing agent and ethylenediaminetetraacetic acid (EDTA, *Sigma Aldrich*) as complexing agent. 0.001% by volume of polyethylene glycol (PEG, M_w 400, *Sigma Aldrich*) was added as surfactant and the pH of the solution was adjusted by dropping 1 M sodium hydroxide (NaOH, *Carlo Erba reagents*) solution.

In order to optimize the electroless deposition process, a randomized full factorial design of experiment (DoE) was set by Minitab software. Four predictor variables have been chosen: (i) the bath temperature (in the range 40–60 °C), (ii) pH (13–13.5), (iii) the concentration of EDTA (0.12–0.24 M), and (iv) the concentration of the reducing agent $C_2H_2O_3$ (0.1–0.4 M). Since two different values were associated to each variables, the DoE campaign is composed of 4 factors and 2 levels resulting in 16 combinations, as reported in Table 1. Each setting was repeated three times for a total of 48 experiments. Samples were immersed in the electroless solution for 35 min and after deposition they have been washed in dH_2O and dried in oven at 50 °C for 24 h.

A traditional electroless plating solution using formaldehyde as reducing agent was prepared as reference [26]. Anhydrous copper (II) sulfate was dissolved in distilled water in the concentration of 0.37 M. Formaldehyde solution (37 wt. % in H_2O, *Sigma Aldrich*) and EDTA were added in 0.1 M and 0.12 M concentration, respectively. 0.001% by volume of polyethylene glycol (PEG MW 400, *Sigma Aldrich*) was added as surfactant. The pH of the solution was maintained at a value of 13 and adjusted by dropping 1 M sodium hydroxide (NaOH, *Carlo Erba reagents*) solution. The deposition temperature was 50 °C and deposition time 35 min.

Table 1 DoE combinations

RunOrder	Sample	Temperature (°C)	pH	EDTA (M)	Glyoxylic acid (M)
1	a	60	13.5	0.24	0.1
2	b	40	13.5	0.24	0.1
3	c	60	13.0	0.24	0.4
4	d	40	13.0	0.12	0.1
5	e	60	13.5	0.12	0.4
6	f	40	13.5	0.12	0.4
7	g	60	13.0	0.12	0.4
8	h	60	13.0	0.24	0.1
9	i	40	13.5	0.12	0.1
10	j	40	13.0	0.12	0.4
11	k	60	13.5	0.12	0.1
12	l	60	13.0	0.12	0.1
13	m	60	13.5	0.24	0.4
14	n	40	13.0	0.24	0.1
15	o	40	13.0	0.24	0.4
16	p	40	13.5	0.24	0.4

After coating process, samples have been washed in dH_2O and dried in oven at 50 °C for 24 h.

The output factors chosen to analyze the influence of the process parameters were (i) the percentage of substrate coated surface, (ii) the adhesion of the coating (critical loads obtained from scratch test), and (iii) the sheet resistance from electrical measurements. The statistical tool of MiniTab software allowed to evaluate both the most influential factors and the influence/interaction given by the combination of input parameters on the output variables. Moreover, a final optimization function allowed to obtain the set of processing parameters to maximize the coating performances which were used for performing the optimized electroless deposition process.

2.4 Crystalline phase analysis and morphological characterization of coatings

Coated samples were imaged via optical microscopy (OM, *Nikon Epiphot TME*) coupled with an acquisition camera (*Visicam 10.0, VWR-Avantor, Radnor, Pennsylvania, USA*). Image analysis was performed by *ImageJ* software, allowing for the calculation of the percentage of the coated area. The coating morphology of deposited samples was investigated also with scanning electron microscopy (FEG-SEM, *Zeiss LEO Supra 35*, accelerating voltage of 5 kV, secondary electron detector),

coupled with Energy Dispersive Spectroscopy (EDS) (*INCAx-sight, Oxford instruments*).

Phase analysis of relevant Cu coatings was assessed by means of X-ray diffraction (XRD) (*Philips X'Pert 1710*, Cu-Kα radiation $\lambda = 1.5405$ Å, 2θ = 10–80°, step size = 0.020°, time per step = 2 s, scan speed = 0.01°/s). The average crystallite size τ was evaluated by applying Scherrer's Eq. (6):

$$\tau = \frac{K\lambda}{\beta \cos\theta}, \tag{6}$$

where K is the shape factor taken as 0.89, λ is the X-ray wavelength, β is the full width at half maximum (FWHM) expressed in radians, and θ is the Bragg angle [27]. The τ values for the copper coatings were determined from profile analysis of the most intense peak present in the XDR pattern.

The dislocation density (δ) and the average and micro-strain (ε) have been calculated according to Eqs. (7) and (8) [28]:

$$\delta = \frac{1}{(\tau)^2} \tag{7}$$

$$\varepsilon = \frac{\beta}{4tan\theta}. \tag{8}$$

2.5 Electrical measurements and coating adhesion

Electrical performances of coatings were measured performing Van der Pauw method [29]. Four probes were brought into contact with the perimeter of the coating at four points, and an electrical current (I) was injected between two of the probes while measuring the electrical potential (V) between the remaining two probes using a digital multimeter (*Keithley* DMM 2700). By averaging on all probe configurations and using Van der Pauw's formula [29], the sheet resistance R_s (measured in Ohms per square, Ω/sq or Ω/□, equivalent to Ωm/m) was calculated.

The adhesion of the coating was assessed by means of scratch test (*Micro-Combi Tester C.S.M. Instruments, Peseaux, Switzerland*), equipped with a Rockwell C-type conical indenter (200 µm tip radius). Three measurements have been performed for each sample, operating in progressive mode (track length 10 mm, scratch speed 10 mm/min, progressive load 0.01–30 N). Scratch tracks have been analyzed by OM (*Nikon Epiphot TME*) and the critical loads (CL) corresponding to different failure mechanisms have been obtained following the UNI EN 1071–3:2005 standard.

3 Results and discussion

The results of contact angle tests reporting the values calculated for the neat and etched substrate are shown in Fig. 1. The neat substrate is characterized by a hydrophobic behavior (contact angle = 99.3° ± 2.1°) which can be ascribed to a non-polar interaction with water. Indeed, the wettability is a function of the nature and packing of the surface atoms or exposed groups of atoms constituting the solid [30]. Epoxy resins typically have a relatively non-polar molecular structure. The presence of non-polar carbon–carbon and carbon–hydrogen bonds can explain the hydrophobic behavior.

As evident, the KOH alcoholic solution modifies the wettability of the organic surface toward a less hydrophobic behavior with a decrease of 10° (contact angle = 89.3° ± 1.7°) and consequently a polar interaction with water. Polarity plays a crucial role in determining the wettability, because the interfacial tension is largely influenced by the surface energy and it generally affects the adhesion of the deposited coating.

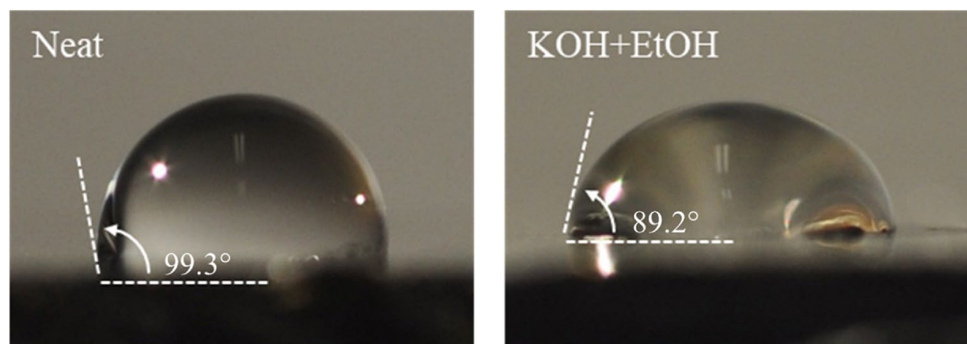

Fig. 1 Water sessile drop on neat and KOH-EtOH-treated epoxy-CFRP samples

Indeed, having a more wettable substrate, and hence with higher surface energy, is beneficial since it can be easily wetted by the pre-activation and activation solutions, resulting in higher adhesion of the copper electroless coating [31].

3.1 Coating morphologies and electrical performances

Figure 2 reports the different coating morphologies obtained with a different combination of electroless plating parameters.

As evident, a variation of process parameters can lead to a completely different morphology. In particular, in some deposition conditions the coating covers the entire surface of the substrate, in others the substrate surface is only partially covered, while in one condition (Fig. 1 n) the coating is barely present.

In Fig. 2, different shades of color of the copper coatings are highlighted. This effect may be due to a combination of two factors: (i) the thickness of the coating, which, as reported in the literature, can cause a more intense and red-brown color in thick coatings and less intense and lighter color in thin coatings [32]; (ii) morphology of the surface, which can cause different scattering of the incident light and therefore a different intensity of coloring. The percentage of covered area is reported in Table 2.

In Fig. 3, the morphologies of the produced coatings acquired with the electron microscopy at higher magnification are shown. Also in this case, all the samples present different microstructures depending on the electroless process conditions. In particular, copper coatings appear to be formed either by round-shaped copper particles having micrometric and sub-micrometric dimension or needle-shaped dendritic copper particles. The electroless deposition of copper from solution occurs at catalytic sites on the substrate surface. In particular, the copper particles nucleate at the most favorable catalytic sites forming aggregates of small crystallites (nuclei) about 25 Å in size [33].

The deposition process goes on autocatalytically and copper deposits on the originally formed nuclei increasing the size of the aggregates until they become

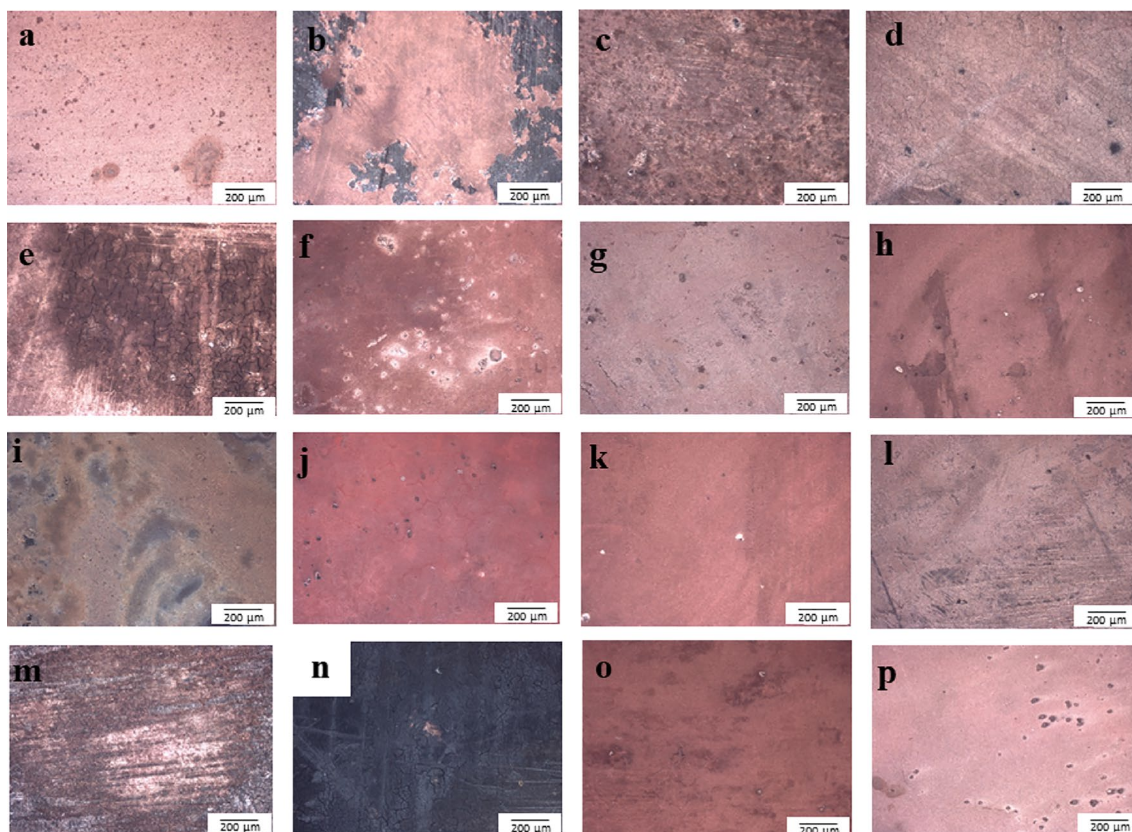

Fig. 2 Optical micrographs showing morphology of electroless-plated specimens in different DoE configurations (a–p) as reported in Table 1

Table 2 Outputs of DoE analysis

Sample	Area (%)	Rs (Ω/☐)	CL1 (N)	CL2 (N)	CL3 (N)
a	99.91 ± 0.10	9.21×10^{-3}	4.82 ± 1.60	14.47 ± 1.83	> 30
b	40.09 ± 3.18	2.86×10^{-2}	–	–	–
c	96.94 ± 1.32	2.75×10^{-2}	–	2.23 ± 0.43	5.98 ± 0.85
d	97.83 ± 1.46	7.87×10^{-2}	2.78 ± 1.13	9.24 ± 1.34	21.11 ± 1.63
e	8.89 ± 1.65	3.16×10^{-2}	1.50 ± 0.57	7.99 ± 2.58	–
f	99.64 ± 0.47	1.87×10^{-2}	2.39 ± 0.09	7.71 ± 3.10	10.74 ± 2.19
g	98.64 ± 0.54	1.58×10^{-2}	2.18 ± 0.98	10.93 ± 0.79	20.45 ± 0.62
h	99.56 ± 0.56	9.10×10^{-3}	9.42 ± 2.09	18.92 ± 3.03	> 30
i	48.70 ± 1.84	3.40×10^{-2}	–	–	–
j	97.31 ± 2.99	8.02×10^{-3}	2.64 ± 1.06	3.95 ± 1.10	15.92 ± 0.13
k	86.51 ± 2.41	1.60×10^{-2}	4.90 ± 1.96	13.50 ± 2.89	22.59 ± 2.01
l	90.68 ± 3.81	2.48×10^{-2}	6.98 ± 1.11	13.31 ± 1.80	23.40 ± 1.14
m	77.31 ± 5.82	3.43×10^{-2}	4.84 ± 2.76	14.62 ± 2.95	24.99 ± 2.89
n	1.24 ± 0.44	–	–	–	–
o	99.96 ± 0.01	9.11×10^{-3}	1.00 ± 0.07	7.94 ± 2.67	15.98 ± 2.21
p	99.46 ± 0.37	9.75×10^{-3}	–	2.23 ± 0.43	5.98 ± 0.85

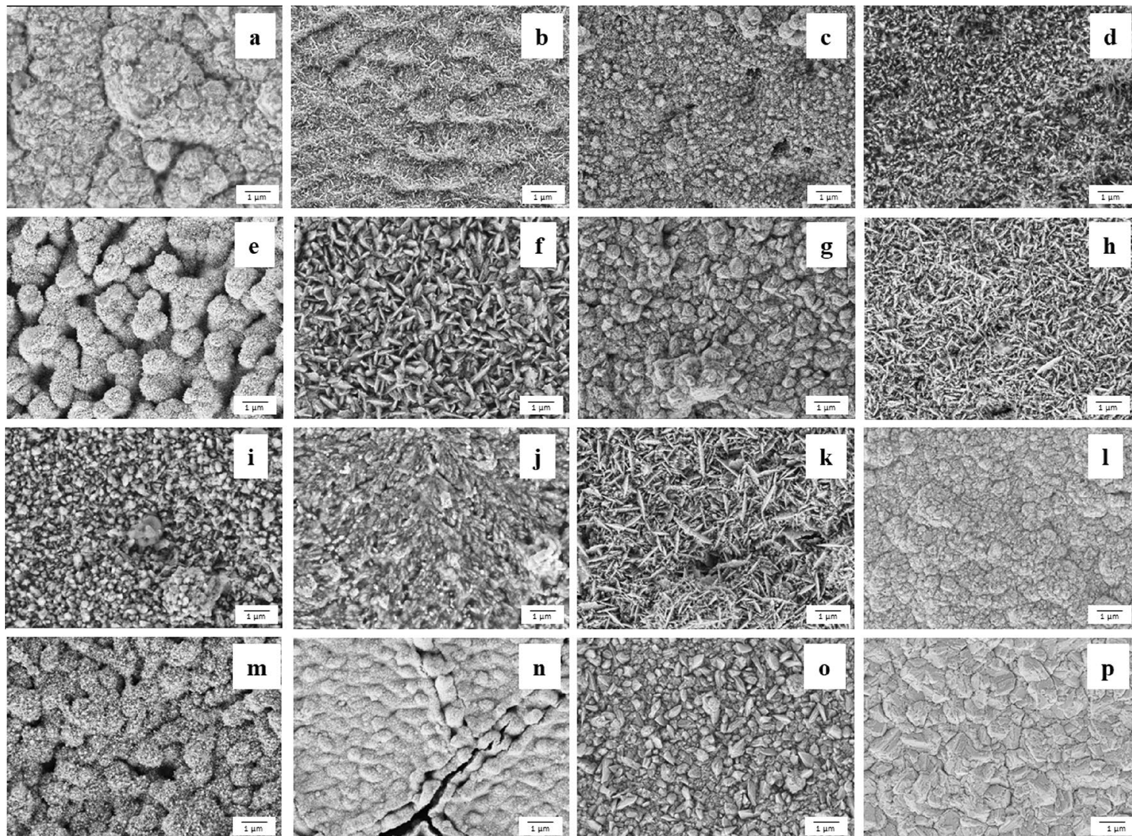

Fig. 3 SEM microstructure of deposited copper coatings in different DoE configurations (a–p) as reported in Table 1

energetically unstable. At this point, a recrystallization process takes place and the unstable aggregates are transformed into grains having micrometric dimensions [33]. Indeed, copper crystals can exhibit anisotropic growth, with a preferential growth along some crystallographic directions. This anisotropy can result in the development of needle-like structures [34]. This behavior is also related to the surface energy of the growing particles. If some orientations have lower energy, they may be favored during growth, leading to the development of needle-like shapes [35]. From the image analysis it is evident that in some specimens, the particle size distribution seems to be more homogeneous than others (e.g., Figure 3, samples i and o). On the other hand, in other specimens (e.g., Figure 3, samples b, c, g, and j) the co-presence of particles with different sizes, thus with a less homogeneous size distribution, can be noted. Moreover, some samples (e.g., sample n where present) show the presence of superficial cracks.

The different microstructure justifies the different electrical behavior shown by the coatings in terms of surface resistance (Rs) obtained from the Van der Pauw test and reported in Table 2. Rs ranges from a minimum value of 8 mΩ/□ to a maximum value of 80 mΩ/□, and are compatible with those found in the literature [36] in which the surface resistance of copper coatings deposited on different substrates has been found in the range 7–20 mΩ/□. Electrical conductivity of copper coating is directly dependent on the thickness of the coating; in particular, a thicker copper coating generally shows higher electrical conductivity compared to a thinner one since thick coatings offer higher pathways for electrons to flow than thin coatings [37]. Coating thickness is directly related to deposition rate which in turn depends on deposition process parameters such as immersion time, pH, and temperature of the electroless bath [20, 25]. Moreover, the surface finish of the coating can influence the electrical conductivity. Smoother surfaces having low roughness tend to conduct better presenting low electrical resistance [38]. In our case, we believe that the difference in the electrical performances should be ascribed to both different coating thickness and microstructure.

3.2 Adhesion of the coating-substrate system

Scratch tests were carried out on all specimens in order to identify the critical loads. Figure 4 reports a representative sample showing the failure mode of the coating at the corresponding critical loads analyzed with the optical microscope.

All samples show, as the load increases, the formation of parabolic cracks or "fish scales" having the concavity in the same direction of the indenter advancement. This first failure, called conformal cracking, consisting in the cohesive cracking of the coating, has been taken as first Critical Load, CL1. Parabolic cracks form as the ductile copper layer tries to fit the deformation of the scratch track. Indeed, as the scratch tip slides on the surface, the coating breaks due to the bending stress imposed in front of the indenter creating cracks which are successively flattened by the passage of the indenter due to the ductile nature of the copper coating. At higher loads (CL2), the CFRP substrate begins to fail, generating cracks with a paraboloid shape having concavity in the opposite direction to that of the indenter. Parabolic cracks are caused by the brittle nature of the substrate which, under high shear forces, breaks down [39, 40]. This failure mode is called *tensile cracking* and the coating fails following the back of the indenter [39, 41, 42] originating the cracks. By further increasing the load, the coating is completely removed from the substrate during the passage of the indenter (CL3) resulting in the complete

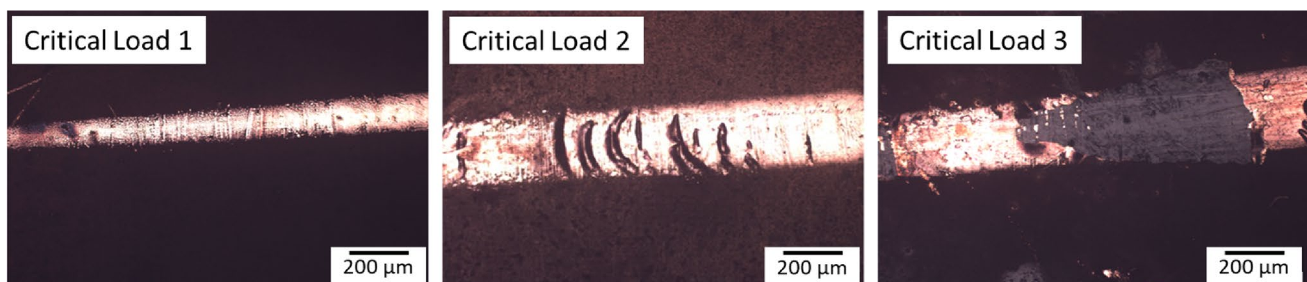

Fig. 4 Representative failure modes of copper coating during scratch test

and continuous exposure of the substrate inside the scratch track. It has to be noted that some samples did not show a CL3 as the maximum applied force during the test (30 N) was not enough to determine the complete removal of the coating exposing the substrate, meaning that the adhesion of the coating-substrate system was high.

3.3 Optimization of the electroless plating processing parameters (DoE)

Once the tests were carried out, the resulting values were used as the output of the process as a function of the input. In this way, by performing the statistical analysis through MiniTab software it was possible to determine the most influential factors for each individual output variable. In particular, the Pareto's charts were generated and are shown in Fig. 5, highlighting the most significant input variables (i.e., those that most influence the entire process as a function of each output variable) prioritizing which factors to focus on for further optimization.

In the charts, the factors (terms) are plotted on a bar chart in descending order of their impact (effect). The red line (α-level) represents a threshold value, calculated by the software, where the factors located to its right are influential in the process. On the other hand, those to the left of the threshold value are not influential and can therefore be omitted in the DOE analysis. As clear from the Pareto's charts for all the outputs, the only influential factors are the temperature of the electroless bath and the combined effect

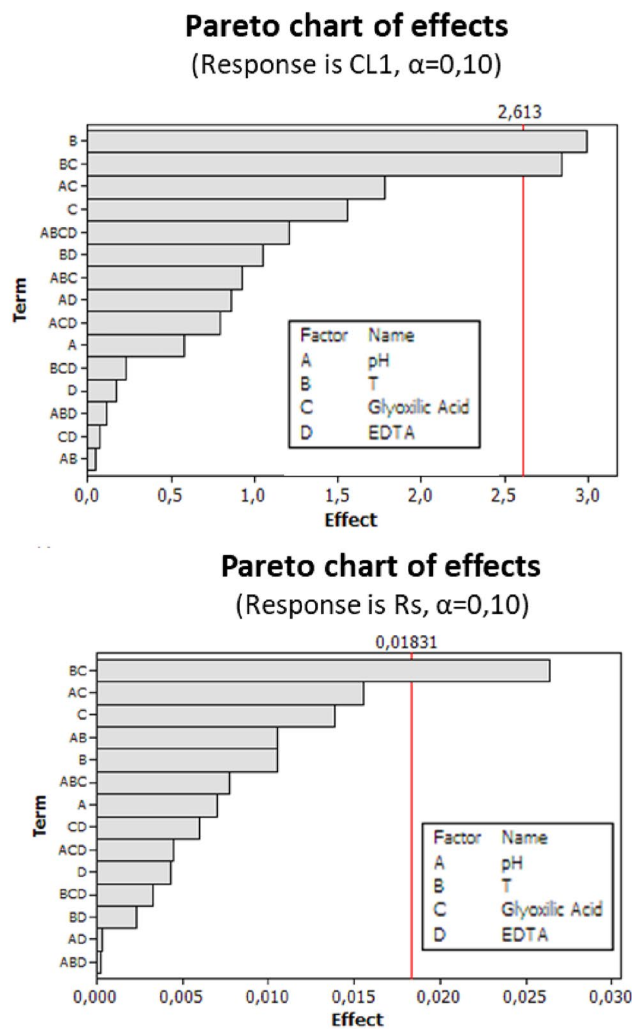

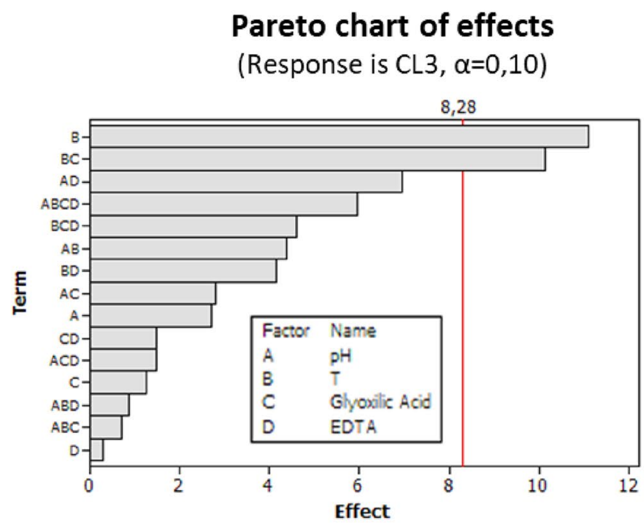

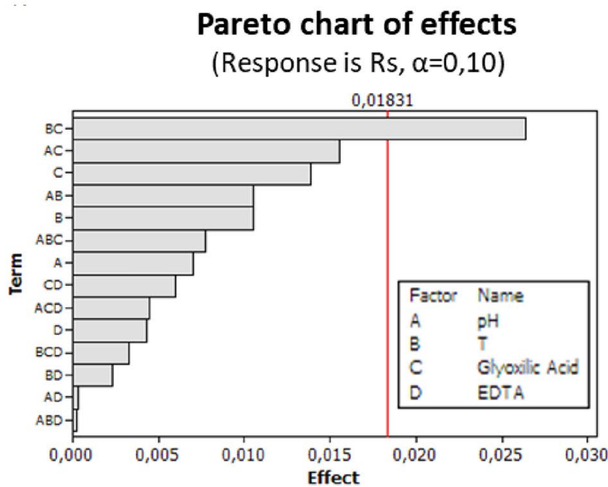

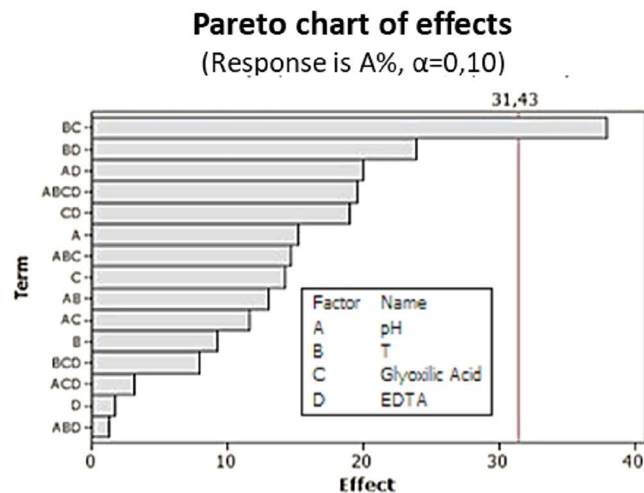

Fig. 5 Pareto charts for CL1, CL3, Rs, and covered area

of temperature and the concentration of the reducing agent glyoxylic acid. Hence, the concentration of the glyoxylic acid and the temperature of the electroless bath were considered as the significant input factors and used to generate the contour plots, which are colored maps where the response (output value) is represented by lines and/or curves as function of to two variables. In Fig. 6, the contour plots for the defined outputs as function of the influential processing parameters ($C_2H_2O_3$ and Temperature) are shown. Those plots allow for the optimization of all the considered outputs determining the set of values suitable to optimize the entire electroless deposition process and therefore obtaining the best performing coating.

Indeed, the MiniTab software offers a multi-objective optimization function in which the functions, which are the considered outputs (i.e., % Area, CL1, CL2, CL3, and Rs), can be maximized (or minimized in the case of Rs) to achieve an optimized deposition process. The multi-objective optimization function has provided a new set of process parameters reported in Table 3 which were used to deposit a new batch of copper electroless-plated samples.

The obtained optimized samples present a very well and homogeneous coating structure, as displayed in Fig. 7, which completely covers the entire substrate surface.

In Fig. 8a, the optimized coating morphology acquired with the electron microscopy is reported and compared to that of coating deposited with the formaldehyde bath in Fig. 8b. As evident, the optimized coating presents a dense and homogeneous

Table 3 Optimized processing values for copper electroless plating on CFRP substrates

Process parameter	Value
pH	13.15
Temperature	60 °C
Glyoxylic acid	0.1 M
EDTA	0.165 M

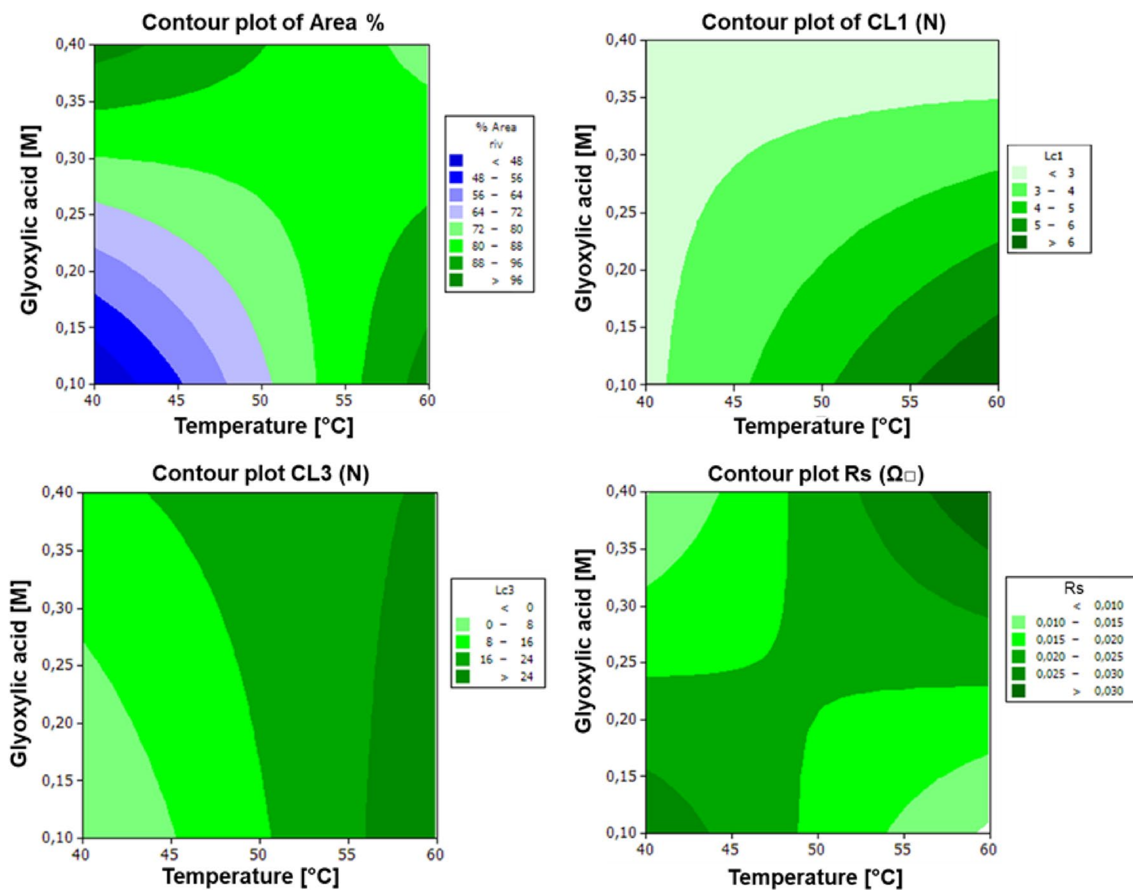

Fig. 6 Contour plots of Area %, Critic load 1 (CL1), Critic load 3 (CL3), and surface resistance, as function of concentration of glyoxylic acid and temperature

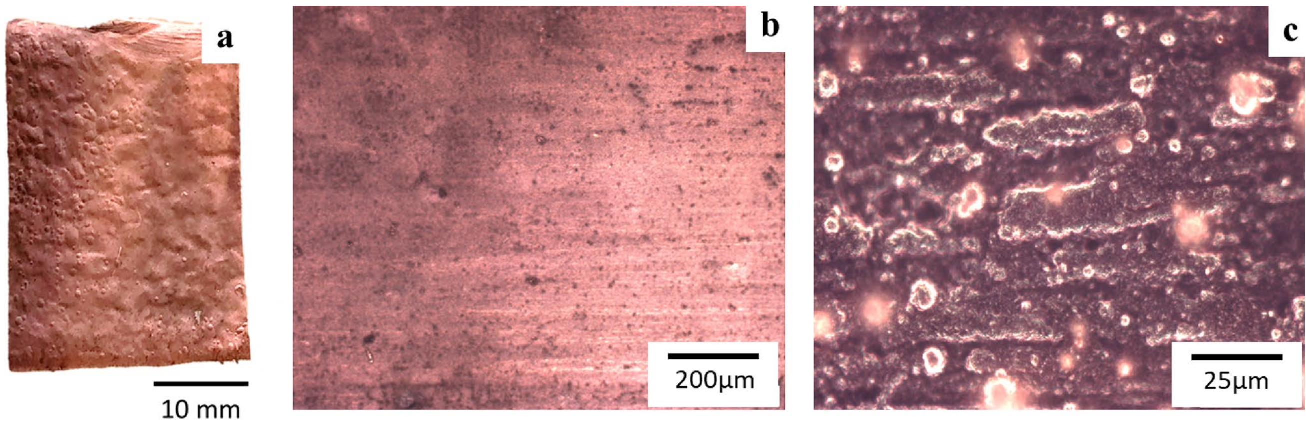

Fig. 7 **a** Picture of optimized copper electroless-plated CFRP sample, **b** low-magnification optical micrograph, **c** high-magnification optical micrograph

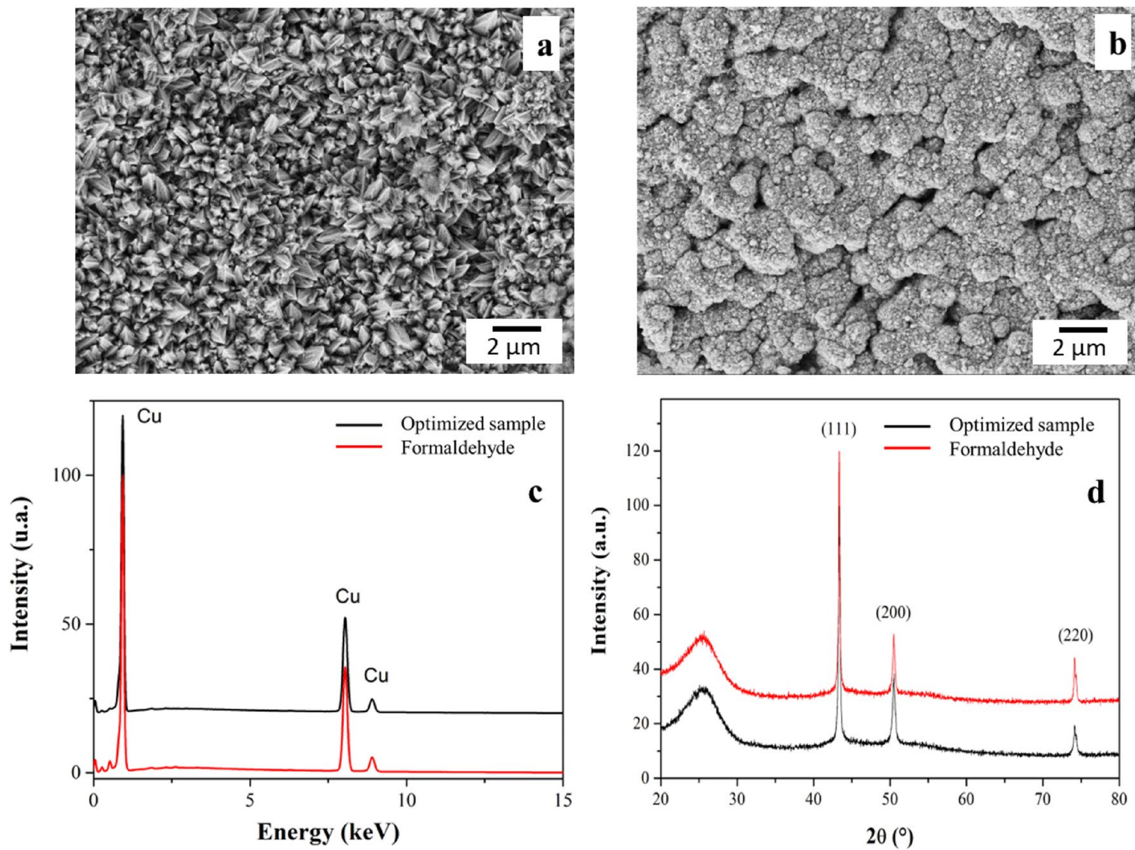

Fig. 8 SEM micrographs of (**a**) optimized and (**b**) formaldehyde reference coating, EDS spectra (**c**), and XRD patterns (**d**)

structure, no presence of cracks was detected, and the elemental analysis (EDS in Fig. 8c) confirmed the purity of the coating as the only detected signals are those ascribable to the copper. Even if both compared samples share the same composition, the coating morphology is quite different.

The formaldehyde sample presents a microstructure composed of round-shaped copper particles

having micro- and nano-dimension, while, on the other hand, the optimized sample presents a microstructure showing dendritic needle-shaped copper particles. Moreover, the formaldehyde sample shows some surface cracks which can be related to the deposition time and the microstructure evolution of copper film [43]. These differences could explain the higher adhesion of the optimized coating. The XRD patterns for the optimized sample and the reference one are compared in Fig. 8d. Both samples show the typical hump at $2\theta = 25°$ ascribable to the amorphous phase of the CFRP substrate (which is mostly made of epoxy resin) and the reflections observed on the diffractogram at 2θ angles of 43.31, 50.45, and 74.12° are those typical of face-centered cubic structure of copper as confirmed by the reference pattern JCPDS 85–1326.

The average crystallite size calculated by applying Scherrer's equation for the optimized sample is 35.9 nm, while the crystallite size for the reference coating, obtained using formaldehyde as reducing agent, is 20.6 nm. It is know that smaller crystallites typically indicate higher energy grain boundaries and greater surface area which generally traduces in a lower electrical conductivity as the higher the grain boundaries, the higher the scatter of the electrons [44]. Indeed, the optimized specimens have a better electrical conductivity due to the improved microstructure of the coating as shown in Table 4, which reports the comparison of results obtained from Van der Pauw test, image analysis, and scratch test. Confirming these results, the dislocation density (δ) and average microstrain (ε) calculated from XRD pattern of optimized sample are $7.76 \times (10^8\ mm^{-2})$ and 2.58×10^{-3}, respectively, while the formaldehyde sample presents a dislocation density value of $23.5 \times (10^8\ mm^{-2})$ and an average micro-strain of 4.51×10^{-3}. A higher dislocation density in the crystal lattice influences both mechanical, electrical, and thermal properties of the coatings. Indeed, dislocations can act as scattering centers for electrons and phonons, decreasing both the electrical and the thermal conductivity of the copper coating [44].

The optimized specimens show also very high values of the critical loads; in particular, the CL1 and the CL3 mean values are higher than those of the reference (formaldehyde sample) confirming the very good adhesion achieved between the coating and the CFRP substrate.

Table 4 Percentage of covered area, scratch test, and electrical test results of optimized and reference samples

Response	Optimized sample	Formaldehyde sample
Area (%)	100	100
CL1 (N)	7.58 ± 0.15	2.535 ± 0.83
CL2 (N)	13.54 ± 2.66	14.74 ± 1.76
CL3 (N)	> 30	22.98 ± 1.49
R_S (Ω/□)	$1.91 \bullet 10^{-2}$	$3.47 \bullet 10^{-2}$

4 Conclusions

In this work, a green electroless copper plating process, substituting formaldehyde with glyoxylic acid as the reducing agent, was optimized for CFRP substrate by employing a four-factor, two-level Design of Experiment. Four process parameters have been selected as factors, namely pH and temperature of the electroless solution, reducing agent concentration (glyoxylic acid), and complexing agent (EDTA) concentration. The different process parameter combinations resulted in vastly different coating morphologies, with surface coverage ranging from 1.2 to 99.9% and different chromatic and visual appearances. The difference in appearance was determined by the coatings' thickness, surface roughness, and morphology of the deposited copper, which are heavily affected by the plating parameters.

Scratch tests and Van der Pauw electrical measurements were carried out to assess and statistically analyze and maximize the coatings' adhesion and electrical conductivity. From the DoE analysis, the bath temperature and the concentration of the reducing agent resulted to be the only statistically significant factors, and a multi-objective optimization was used to determine the optimal parameters to obtain a coating with maximum surface coverage, adhesion, and conductivity (namely pH 13.15, temperature of 60 °C, and reducing and complexing agent concentrations of 0.1 and 0.165 M, respectively).

The optimized coating showed 100% surface coverage, a surface resistivity of 19 mΩ/□, and first and third scratch test critical loads of 7.6 and > 30N, which are higher performances than the reference sample, plated with a standard formaldehyde-based electroless bath from literature. The proposed optimized process, therefore, allows for the coating of complex and electrically insulating substrates with a conductive copper coating without the use of toxic and

environmentally impactful chemicals, representing a greener alternative to the traditional processes. These copper coatings could represent interesting solutions as electrically conductive surface layers in electronics, electromagnetic interference (EMI) shielding, or radiofrequency transmission applications, as well as preferential heat dissipation paths in high-performance (i.e., aerospace) applications.

Acknowledgements

The authors wish to thank Mr. Francesco Rigoli for his precious help during the experimental campaign.

Funding

Open access funding provided by Università degli Studi di Roma Tor Vergata within the CRUI-CARE Agreement.

Data availability

Data are available on request from the authors. The data that support the findings of this study are available from the corresponding author upon reasonable request.

Declarations

Conflict of interest The authors have no conflicts to disclose.

Open Access This article is licensed under a Creative Commons Attribution 4.0 International License, which permits use, sharing, adaptation, distribution and reproduction in any medium or format, as long as you give appropriate credit to the original author(s) and the source, provide a link to the Creative Commons licence, and indicate if changes were made. The images or other third party material in this article are included in the article's Creative Commons licence, unless indicated otherwise in a credit line to the material. If material is not included in the article's Creative Commons licence and your intended use is not permitted by statutory regulation or exceeds the permitted use, you will need to obtain permission directly from the copyright holder. To view a copy of this licence, visit http://creativecommons.org/licenses/by/4.0/.

References

1. C. Nelon, A. Shepard, I. Walker, O. Myers, Transverse curvature characterization of rectangular bistable CFRP laminates with a satellite capturing continuum robotic application. Compos. Struct. **325**, 117565 (2023). https://doi.org/10.1016/j.compstruct.2023.117565
2. M. Bragaglia, V. Pascale, M. Rinaldi, F. Nanni, Silver electroless plating on 3D printed resins via stereolithography: a sustainable solution. Thin Solid Films **757**, 139417 (2022). https://doi.org/10.1016/j.tsf.2022.139417
3. A. Goktas, F. Aslan, A. Tumbul, Nanostructured Cu-doped ZnS polycrystalline thin films produced by a wet chemical route: the influences of Cu doping and film thickness on the structural, optical and electrical properties. J. Sol-Gel Sci. Technol. **75**, 45–53 (2015). https://doi.org/10.1007/s10971-015-3674-8
4. J.B.H. Glenn O. Mallory, 1990 Electroless Plating : Fundamentals And Applications, William Andrew.
5. A. Equbal, N.K. Dixit, A.K. Sood, Int. J. Sci. Eng. Res. **4**, 32–41 (2013)
6. P. Dechasit, W. Treakarnpruk, Ni electroless plating of ABS polymer by palladium and tin-free process. J. Met. Mater. Miner. **21**, 19–27 (2011)
7. M. Krishnan, Electroless plating of copper at a low pH level **37**, 117–124 (1993)
8. M.C. Zhang, E.T. Kang, K.G. Neoh, K.L. Tan, Electroless plating of copper and nickel on surface-modified poly (tetrafluoroethylene) films. J. Electrochem. Soci. (2001). https://doi.org/10.1149/1340916
9. S. Ghosh, Electroless copper deposition: a critical review. Thin Solid Films **669**, 641–658 (2019). https://doi.org/10.1016/j.tsf.2018.11.016
10. L. Bernardini, E. Barbosa, M.F. Charão, N. Brucker, Formaldehyde toxicity reports from in vitro and in vivo studies: a review and updated data. Drug. Chem. Toxicol. **45**, 972–984 (2022). https://doi.org/10.1080/01480545.2020.1795190
11. G. La Torre, T. Vitello, R.A. Cocchiara, C. Della Rocca, Relationship between formaldehyde exposure, respiratory irritant effects and cancers: a review of reviews. Public Health **218**, 186–196 (2023). https://doi.org/10.1016/j.puhe.2023.03.009

12. W.R. Brasch, Formaldehyde-free electroless copper plating solutions, European Patent 0384180A1, application number 90102002.4, 1990.
13. H. Honma, T. Kobayashi, J. Electrochem. Soc. **141**, 730–733 (1994)
14. D.H. Cheng, W.Y. Xu, Z.Y. Zhang, Z.H. Yiao, Electroless copper plating using hypophosphite as reducing agent. Met. Finish. **95**, 34–37 (1997). https://doi.org/10.1016/S0026-0576(97)81804-1
15. F. Yang, B. Yang, B. Lu, L. Huang, S. Xu, S. Zhou, Electrochemical study on electroless copper plating using sodium hypophosphite as reductant. Acta Phys.-Chimica Sin **22**, 1317–1321 (2006). https://doi.org/10.1016/S1872-1508(06)60065-X
16. A.-N. Zheng, Z.-Y. Wang, J.-Q. Yang, L. Jin, F.-Z. Yang, D.-P. Zhan, Advanced Ag nanoparticles for the catalyzation of glyoxylic acid oxidation in through-holes electroless copper metallization. J. Colloid Interface Sci. **648**, 270–277 (2023). https://doi.org/10.1016/j.jcis.2023.05.177
17. L.S. Altynbaeva, A.A. Mashentseva, N.A. Aimanova, D.A. Zheltov, D.I. Shlimas, D.T. Nurpeisova, M. Barsbay, F.U. Abuova, M.V. Zdorovets, Eco-friendly electroless template synthesis of Cu-based composite track-etched membranes for sorption removal of lead(II) ions. Membranes (Basel) **13**, 495 (2023). https://doi.org/10.3390/membranes13050495
18. L. Yu, L. Guo, R. Preisser, R. Akolkar, Autocatalysis during electroless copper deposition using glyoxylic acid as reducing agent. J. Electrochem. Soc. **160**, D3004–D3008 (2013). https://doi.org/10.1149/2.002312jes
19. F. Hanna, Z. Abdel Hamid, A. Abdel Aal, Controlling factors affecting the stability and rate of electroless copper plating. Mater. Lett. **58**, 104–109 (2004). https://doi.org/10.1016/S0167-577X(03)00424-5
20. N. Kulyk, S. Cherevko, C.-H. Chung, Copper electroless plating in weakly alkaline electrolytes using DMAB as a reducing agent for metallization on polymer films. Electrochim. Acta **59**, 179–185 (2012). https://doi.org/10.1016/j.electacta.2011.10.053
21. J.I. Martins, M.C. Nunes, On the kinetics of copper electroless plating with hypophosphite reductant. Surf. Eng. **32**, 363–371 (2016). https://doi.org/10.1179/1743294415Y.0000000066
22. J.H. Huang, P.S. Shih, V. Renganathan, S.J. Gräfner, Y.A. Chen, C.H. Huang, C.L. Kao, Y.S. Lin, Y.C. Hung, C.R. Kao, Development of high copper concentration, low operating temperature, and environmentally friendly electroless copper plating using a copper—glycerin complex solution. Electrochim. Acta **425**, 140710 (2022). https://doi.org/10.1016/j.electacta.2022.140710
23. Y. Shacham-Diamand, V. Dubin, M. Angyal, Electroless copper deposition for ULSI. Thin Solid Films **262**, 93–103 (1995). https://doi.org/10.1016/0040-6090(95)05836-2
24. K. Pawar, P. Dixit, A critical review of copper electroless deposition on glass substrates for microsystems packaging applications. Surf. Eng. **38**, 576–617 (2022). https://doi.org/10.1080/02670844.2022.2142002
25. P. Balaramesh, P. Venkatesh, S. Rekha, Influence of imidazole and benzotriazole on electroless copper plating. Surf. Eng. **30**, 552–556 (2014). https://doi.org/10.1179/1743294414Y.0000000281
26. J. Dumesic, J.A. Koutsky, T.W. Chapman, The rate of electroless copper depositionby formaldehyde reduction. J. Electrochem. Soc. **121**, 1405 (1974). https://doi.org/10.1149/1.2401698
27. M. Bragaglia, F.R. Lamastra, M. Tului, L. Di Gaspare, A. Notargiacomo, M. Valentini, F. Nanni, Low temperature sputtered ITO on glass and epoxy resin substrates: influence of process parameters and substrate roughness on morphological and electrical properties. Surf. Interfaces **17**, 1–7 (2019). https://doi.org/10.1016/j.surfin.2019.100365
28. Z. Aba, A. Goktas, A. Kilic, Characterization of Zn1-xLaxS thin films; compositional, surface, optical, and photoluminescence properties for possible optoelectronic and photocatalytic applications. J. Sol-Gel Sci. Technol. **109**, 260–271 (2024). https://doi.org/10.1007/s10971-023-06273-w
29. L.J. van der PAUW, 1991 A METHOD OF MEASURING SPECIFIC RESISTIVITY AND HALL EFFECT OF DISCS OF ARBITRARY SHAPE, in: Semicond. Devices Pioneer. Papers, WORLD SCIENTIFIC: pp. 174–182. https://doi.org/10.1142/9789814503464_0017.
30. N. Giovambattista, P.G. Debenedetti, P.J. Rossky, Effect of surface polarity on water contact angle and interfacial hydration structure. J. Phys. Chem. B **111**, 9581–9587 (2007). https://doi.org/10.1021/jp071957s
31. Y. Wang, C. Bian, X. Jing, Adhesion improvement of electroless copper plating on phenolic resin matrix composite through a tin-free sensitization process. Appl. Surf. Sci. **271**, 303–310 (2013). https://doi.org/10.1016/j.apsusc.2013.01.188
32. N.N.C. Isa, Y. Mohd, M.H.M. Zaki, S.A.S. Mohamad, Characterization of copper coating electrodeposited on stainless steel substrate. Int. J. Electrochem. Sci. **12**, 6010–6021 (2017). https://doi.org/10.20964/2017.07.58
33. R. Sard, The nucleation, growth, and structure of electroless copper deposits. J. Electrochem. Soc. **117**, 864 (1970). https://doi.org/10.1149/1.2407658

34. R. Junginger, G. Elsner, On the texture of electroless copper films. J. Electrochem. Soc. **135**, 2304–2308 (1988). https://doi.org/10.1149/1.2096258
35. C. Yan, D. Xue, A modified electroless deposition route to dendritic Cu metal nanostructures. Cryst. Growth Des. **8**, 1849–1854 (2008). https://doi.org/10.1021/cg700851x
36. G.T. Azar, D. Fox, Y. Fedutik, L. Krishnan, A.J. Cobley, Functionalised copper nanoparticle catalysts for electroless copper plating on textiles. Surf. Coatings Technol. (2020). https://doi.org/10.1016/j.surfcoat.2020.125971
37. M. Radoeva, B. Radoev, Ohm resistivity of electroless copper layers as a function of their thicknesses. J. Mater. Sci. **30**, 2215–2219 (1995). https://doi.org/10.1007/BF01184563
38. A. Javidjam, M.H. Hekmatshoar, L. Hedayatifar, S.N.K. Abad, Effect of surface roughness on electrical conductivity and hardness of silver plated copper. Mater. Res. Express. **6**, 036407 (2018). https://doi.org/10.1088/2053-1591/aaf4c5
39. H. Jiang, R. Browning, H.J. Sue, Understanding of scratch-induced damage mechanisms in polymers. Polymer (Guildf). **50**, 4056–4065 (2009). https://doi.org/10.1016/j.polymer.2009.06.061
40. M. Hamdi, X. Zhang, H.-J. Sue, Fundamental understanding on scratch behavior of polymeric laminates. Wear **380–381**, 203–216 (2017). https://doi.org/10.1016/j.wear.2017.03.024
41. R.S. Hadal, R.D.K. Misra, Mater. Sci. Eng.: A **398**, 252–261 (2005). https://doi.org/10.1016/j.msea.2005.03.028
42. T. Sander, S. Tremmel, S. Wartzack, A modified scratch test for the mechanical characterization of scratch resistance and adhesion of thin hard coatings on soft substrates. Surf. Coatings Technol. **206**, 1873–1878 (2011). https://doi.org/10.1016/j.surfcoat.2011.08.035
43. C. Dehchar, I. Chikouche, R. Kherrat, A. Sahari, A. Zouaoui, A. Merati, Electroless copper deposition on epoxy glass substrate for electrocatalysis of formaldehyde. Mater. Lett. **228**, 439–442 (2018). https://doi.org/10.1016/j.matlet.2018.06.076
44. L. Lu, Y. Shen, X. Chen, L. Qian, K. Lu, Ultrahigh strength and high electrical conductivity in copper. Science (2004). https://doi.org/10.1126/science.1092905

Publisher's Note Springer Nature remains neutral with regard to jurisdictional claims in published maps and institutional affiliations.